Mesoporous Films

Thermally Stable Nanocrystalline γ-Alumina Layers with Highly Ordered 3D Mesoporosity**

*Monika Kuemmel, David Grosso, Cédric Boissière, Bernd Smarsly, Torsten Brezesinski, Pierre A. Albouy, Heinz Amenitsch, and Clement Sanchez**

Mesostructured materials can be obtained by combining ionic surfactants[1] or block copolymers[2] with the synthesis of metallic oxides through soft chemistry. Amongst the non-silicate mesoporous materials, alumina is very attractive since the Al_2O_3 has perfectly controlled mesoporosity associated with hardness, hydrolytic stability, amphoteric character, and thermal stability of the γ-transition-oxide phases. Indeed, alumina offers a range of possibilities for applications in ultrafiltration of salts,[3] as an adsorbent in environmental cleanup,[4] as an automobile exhaust catalyst,[5] as a heterogeneous catalyst support for hydrodechlorination,[6] and in petroleum refinement.[7] In state-of-the-art syntheses, ordered mesoporosity has been reported for boehmite,[8] gibbsite,[9] and alumina[2,5,10] through the template approach, and also by porogen bead inclusion,[11] by ordered mesoporous carbon (CMK) nanocasting,[12] and by anodization.[8a] However, none of these materials combines pure crystalline γ-Al_2O_3 of high thermal stability with a well-ordered porosity that has a narrow distribution and is adjusted on the mesoscopic scale.

Herein, we describe the preparation and characterization of nanocrystalline γ-Al_2O_3 layers with contracted face-centered cubic (fcc) mesoporosity that are stable up to 900 °C. These coatings were prepared by combining the block copolymer structuring approach[13] and the evaporation-induced self-assembly (EISA) method associated with layer deposition,[14] which has already led to mesoporous silica,[11] transition-metal oxide,[15] and even perovskite[16] layers. Here we show that such fcc-mesostructured alumina layers can be prepared reproducibly by a simple method by which one may

- adjust the mesopore dimension with a relatively narrow size distribution,
- tune the nature of the oxide framework between amorphous alumina to fully nanocrystalline γ-Al_2O_3,
- create up to 55 % volume of open porosity at 900 °C,
- adjust the layer thickness up to 1000 nm, and
- tune the refractive index from 1.19 to that of pure alumina (measured at 700 nm in a dry atmosphere).

These layers can thus find potential applications as low-refractive-index optical thin films or in the various domains mentioned above if used as coatings. In addition, we present the first fcc mesostructure ever reported for a non-silica system. The complete study of such a layer is assessed by 2D small-angle X-ray scattering (SAXS), transmission electron microscopy (TEM), electronic diffraction, atomic force microscopy (AFM), and ellipsometric porosimetry (EP). Finally, explanations for the high-temperature stability are given.

Layers (300-nm thick) of nanocrystalline γ- Al_2O_3 with optical quality were prepared as reported in the Experimental Section. Figure 1 shows the evolution of in situ 2D SAXS patterns obtained during thermal treatment. Indexation of the diffraction spots (Figure 1 b) reveals that the initial structure at 25 °C is a perfect fcc structure with lattice parameters of 36 and 60 nm when the KLE22 (Figure 1 a) and KLE23 block copolymer templates (Figure 1 d) are used, respectively (for KLE composition, see the Experimental Section). The diffraction rings (Figure 1 c, inset) are characteristic of the preferential monoorientation with the [111] direction normal to the surface (direction of shrinkage). Figure 1 c shows the diffraction pattern of a KLE22-templated alumina film calcined for 20 min at 900 °C. For clarity, diffraction points

[*] M. Kuemmel, Dr. D. Grosso, Dr. C. Boissière, Dr. C. Sanchez
Chimie de la Matière Condensée, UMR UPMC-CNRS 7574
4 place Jussieu, 75252 Paris 05 (France)
Fax: (+33) 1-4427-4769
E-mail: clems@ccr.jussieu.fr
Dr. B. Smarsly, T. Brezesinski
Max Planck Institute of Colloids and Interfaces
Research Campus Golm, 14424 Potsdam (Germany)
Dr. P. A. Albouy
Laboratoire de Physique des Solides
Université Paris-Sud, 91405 Orsay (France)
Dr. H. Amenitsch
Institute of Biophysics and X-ray Structure Research
Austrian Academy of Sciences
Steyrergasse 17/VI, 8010 Graz (Austria)

[**] We thank the European Network of Excellence FAME and the CNRS for funding, and Dr. Markus Antonietti from the Max Planck Institute of Colloids and Interfaces (Golm, Germany) for providing the KLE block copolymers. D. Jalabert from the Center of Electronic Microscopy of Orléans (France) is acknowledged for TEM and HRTEM analyses.

Supporting information for this article is available on the WWW under http://www.angewandte.org or from the author.

 DOI: 10.1002/ange.200500037

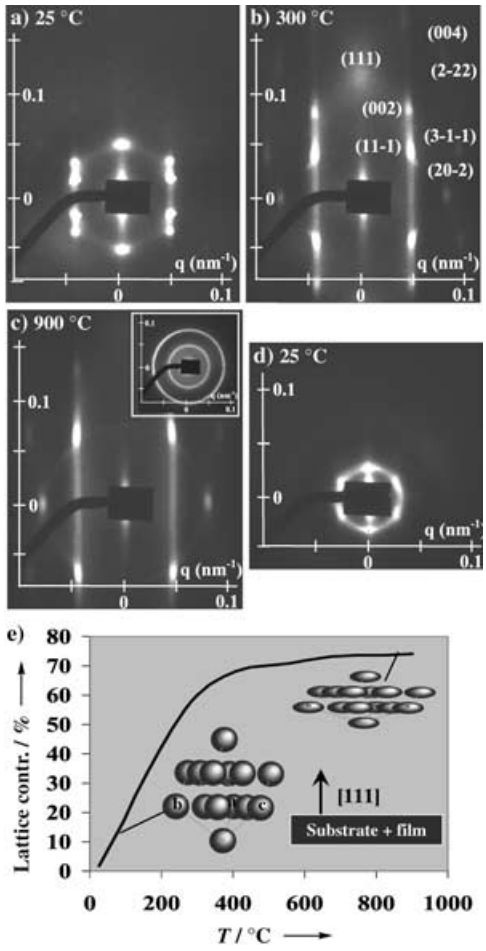

Figure 1. a)–c) 2D SAXS patterns of KLE22-templated alumina layers treated at various temperatures. c) Inset: diffraction rings. d) 2D SAXS patterns of KLE23-templated alumina layer at room temperature. e) Evolution of the fcc lattice contraction in the direction normal to the layer surface ([111] direction of the fcc domains) versus temperature.

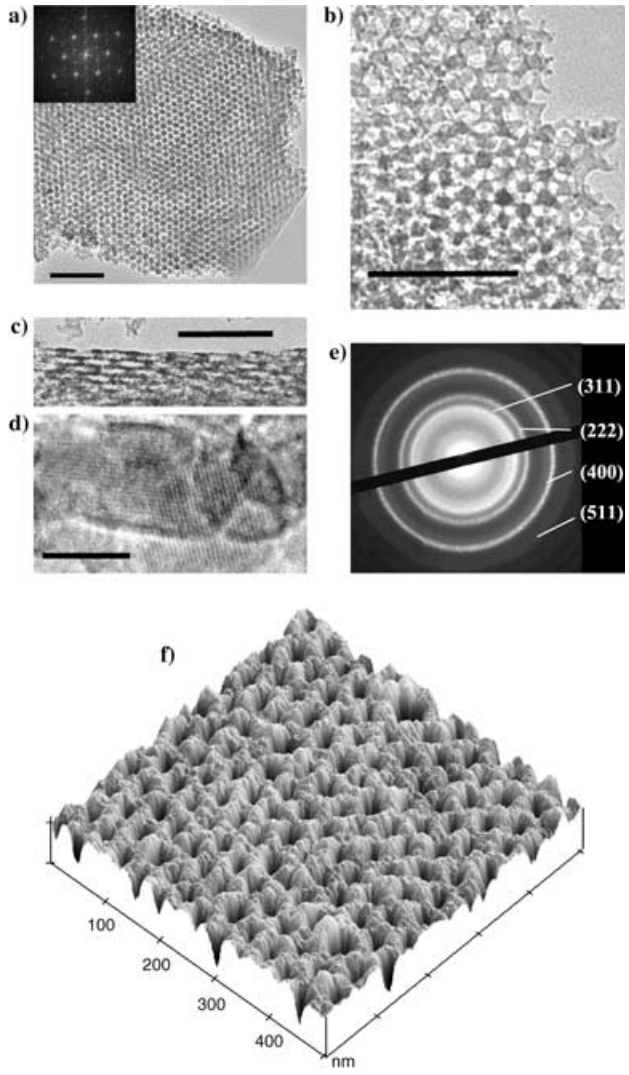

Figure 2. Electronic microscopy and diffraction investigations of KLE22-templated alumina layers treated at 400 °C (a) and at 900 °C (b–e). AFM topography of KLE23-templated layer treated at 900 °C (f). Images of the contracted fcc domains are given in the [111] zone axis for (b) and (c) and in the [1-10] zone axis for (c). Scale bars: 50 nm for (a) and (b), 25 nm for (c), and 5 nm for (d).

corresponding to these contracted systems are indexed with the original fcc structure.

Despite the significant lattice contraction found in Figure 1, the diffraction peaks are still very intense and well-resolved. The initial contraction of 68 % took place between room temperature and 400 °C, while the remaining 6 % occurred between 400 and 900 °C. The cubic structure is clearly confirmed by TEM analysis (see Figure 2), where the [111] view plane of the contracted fcc arrangement of pores exhibits the expected hexagonal arrays (Figure 2 a and b). The side view of the film in Figure 2 c confirms the fcc-based structure. It also reveals that pores are highly anisotropic as a result of the high degree of contraction induced by the thermal treatment. Energy-dispersive X-ray analysis confirmed that the whole mesostructure contains only Al and O elements. The surfaces of the thin films were probed by AFM, and the image obtained for the corresponding KLE23-templated film treated at 900 °C is shown in Figure 2 f.

AFM observations indicated that the porosity is open to the atmosphere through a hexagonal array of well-calibrated circular pores of average diameter 23 nm (see the Supporting Information). This topography is characteristic of the [111] plane from the contracted fcc arrangement of spherical pores with dimension similar to the size of templating micelles. The average pore depth was probed at 6 ± 1 nm. The HRTEM image (Figure 2 d) shows crystalline nanoparticles of around 5 nm in diameter with reticular distances corresponding to the (311) and (222) d spacing of the γ-Al_2O_3 phase. The corresponding diffraction pattern of the latter very stable alumina phase was also observed by electronic diffraction (Figure 2 e). Films treated for 20 min at 400 °C show no crystallinity, which suggests that the alumina framework is amorphous and crystallizes into γ-Al_2O_3 progressively from 400 to 900 °C. Electronic diffraction (see the Supporting Information) revealed that upon treatment above 900 °C, the d spacing slightly decreased, and diffraction spots clearly appeared on the diffraction rings. This finding is attributed to the γ-Al_2O_3 particles coalescing into larger crystalline particles of δ-Al_2O_3

through the combined effect of γ-to-δ phase transformation and diffusive sintering of nanoparticles. This transformation is accompanied by a degradation of the mesostructure. δ-Al_2O_3 is the transition alumina phase lying between γ- and α-Al_2O_3 (corundum). Before thermal treatment the inorganic network is probably composed of Al^{3+}-based polymeric species from the initial slightly acidic aqueous solution (hydrated gibbsite or boehmite phases).[9a] Starting at 400 °C, progressive crystallization into transition alumina phases occurs. At 900 °C the structure is that of γ-Al_2O_3 (*Fd3m* lacunar spinel) with the lattice parameter $a = 7.9$ Å. Above 900 °C, the original lattice distorts into δ-Al_2O_3 as a result of the increase in Al atoms located in octahedral sites. Such a particular sequence of transformation is usually observed during thermal decomposition of the boehmite precursor.[17]

It is well known that pore morphology is difficult to assess in thin films as a result of the very low quantity of material. The actual KLE22 and KLE23 block copolymer templates form spherical organic domains that have a given diameter of around 10 and 20 nm, respectively.[18] It is evident from the lattice contraction (Figure 1) that, after thermal treatment, pores adopt an ellipsoidal disk morphology with a large axis (d_w) close to the initial dimension of the porogen template, while the small axis depends on the contraction. For instance, an aspect ratio of 4 can be roughly measured in Figure 2c. Such pore dimensions, their interconnection, and therefore the diffusion through the layer were investigated by EP (see the Supporting Information).[19] Isotherms of water adsorption–desorption of KLE22- and KLE23-templated layers thermally treated at 900 °C are given in Figure 3. A volume of water up to 55 % is adsorbed inside the matrix at high relative humidity, which corresponds to the volume of accessible porosity. The main capillary condensation takes place at narrow relative pressure domains above 0.6, which suggests that mesopores of both layers are relatively well-calibrated. Very little water is adsorbed at low relative pressure, therefore only a tiny fraction of the porosity is expected to consist of micropores. Capillary condensation takes place at higher relative pressures when KLE23 is used because of the wider pores obtained with such a template. The pore-size distributions presented in Figure 3 are evaluated using Kelvin's equation modified for ellipsoidal pores (see the Supporting Information). The characteristics of the porosity are given in Table 1.

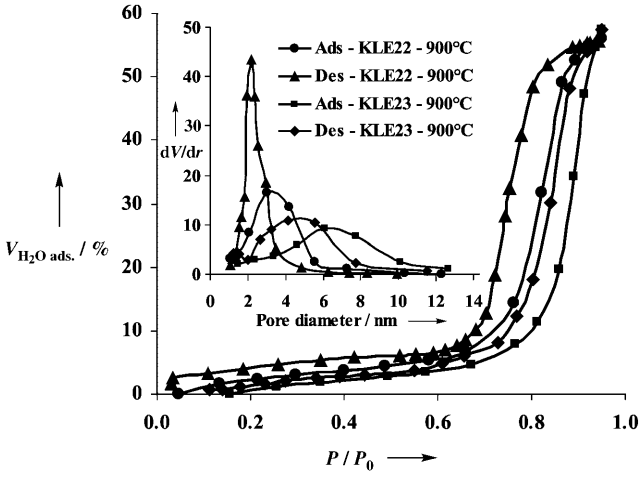

Figure 3. Water adsorption–desorption isotherms obtained from EP measurements performed on KLE22- and KLE23-templated alumina layers thermally treated at 900 °C. Inset: corresponding pore-size distributions deduced from the adsorption and desorption branches.

Table 1: Crystalline phase, pore volume *P*, pore small axis D_s deduced from adsorption, pore wide diameter D_w deduced from pore anisotropic factor, and interconnection diameter D_i deduced from desorption of KLE22- and KLE23-templated alumina layers depending on treatment temperature *T*.

Film	*T* [°C]	Phase	*P* [%]	D_s [nm]	D_w [nm]	D_i [nm]
AlKLE22	900	γ-Al_2O_3	55	3.3 ± 1	13 ± 4	2 ± 0.5
AlKLE22	940	δ-Al_2O_3	55	5 ± 2	–	–
AlKLE23	900	γ-Al_2O_3	55	6 ± 2	24 ± 5	5 ± 2

After crystallization into γ-Al_2O_3, the pore dimensions deduced from the isotherm adsorption branches are 3.3 and 6 nm for KLE22-and KLE23-templated structures, respectively. Both dimensions correspond to the smaller axes of the ellipsoidal pores, whereas their corresponding large axes (13 and 24 nm, respectively) are deduced from the pore aspect ratio. These results are in agreement with the TEM and AFM investigations and confirm the ellipsoidal-disk morphology of the pore, as expected when spherical shapes are unidirectionally contracted. The slightly greater value of the larger pore diameter is related to the matrix densification (crystallization and sintering) at high temperatures. The pore-size distributions become wider after transformation into δ-Al_2O_3 at 940 °C, as a result of the slight degradation of the mesoporous order already observed by TEM and electronic diffraction. No clear pore-size distribution could be deduced from the desorption branches. The dimensions deduced from the desorption branches are characteristic of the pore interconnection (bottleneck) that limits the diffusion of species within the porosity and delays the desorption. Both γ-Al_2O_3 mesostructures present pore-size distributions from desorption branches that are smaller than the dimension of their primary disk-shaped pores (that is, 2 and 5 nm for KLE22 and KLE23, respectively, deduced from the ellipsoidal geometry model). According to the fcc initial structure, every ellipsoidal-disk pore has six first neighbors since they are in an octahedral environment. The pores hold three interconnecting windows on each face of the disk as a result of contraction. A scheme of such an open, contracted-fcc mesostructure is represented in Figure 4.

In summary, the ability to stabilize γ-Al_2O_3 nanoparticles into a well-ordered three-dimensional mesostructured network is first attributed to the stability of the KLE22 template above the dehydration temperature of the inorganic phase. When the treatment reaches the KLE decomposition temperature at 350 °C, the amorphous inorganic dehydrated framework is rigid enough to prevent the mesostructure from collapsing. Above 400 °C, progressive crystallization by nucleation and growth slowly takes place, as expected for transition alumina phases, but the diffusive sintering usually responsible for the collapse of the transition-metal-oxide

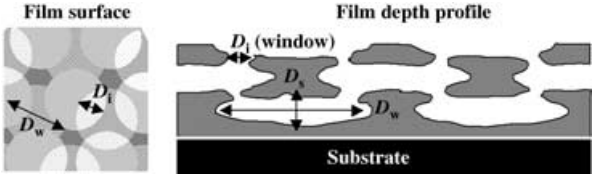

Figure 4. Scheme of the contracted-fcc nanocrystalline mesoporous film structure showing the corresponding surface ([111] zone axis) and depth-profile views ([1-10] zone axis). Pores of small and large diameter (D_s and D_w) with their interconnection dimension (D_i) are represented with respect to the arrangement of the disk-shaped pores.

mesostructure[20] is limited here by the spatial separation of the inorganic walls associated with the ordered mesostructure. The final nanocrystalline mesostructure is composed of ellipsoidal disk-shaped pores, which result from the unidirectional contraction associated with organic decomposition and the densification of the inorganic walls. The porosity (50% volume) is composed of well-calibrated mesopores and is accessible through interconnecting windows 2 or 5 nm in diameter, which is fixed by the template size.

Experimental Section

Isotropic solutions were prepared by dissolving $AlCl_3{\cdot}6\,H_2O$ precursor (0.3 g) and block copolymer KLE22 (BH_{79}-*b*-EO_{89}) or KLE23 (BH_{320}-*b*-EO_{568}) (BH = hydrogenated poly-*b*-butadiene-coethylene; EO = polyoxyethylene) template (0.06 g) in ethanol (5 mL) and H_2O (0.2 mL; 0.1 M NH_4OH). The solutions were aged for 7 days at room temperature before deposition. Films were prepared by dip-coating at a constant relative humidity of 30%. Amorphous ordered mesoporous layers were obtained at 400 °C (10 °C min^{-1} under air) whereas γ- and δ-Al_2O_3 nanocrystalline mesoporous networks were formed at 900 and 940 °C, respectively.

Received: January 5, 2005
Revised: March 22, 2005
Published online: June 24, 2005

Keywords: aluminum · mesoporous materials · nanostructures · template synthesis · thin films

[1] C. T. Kresge, M. E. Leonowicz, W. J. Roth, J. C. Vartuli, J. S. Beck, *Nature* **1992**, *359*, 710 – 712.
[2] P. Yang, D. Zhao, D. I. Margolese, B. Chmelka, G. Stucky, *Nature* **1998**, *396*, 152 – 155.
[3] J. Schaep, C. Vandecasteele, B. Peeters, J. Luyten, C. Dotremont, D. Roels, *J. Membr. Sci.* **1999**, *163*, 229 – 237.
[4] Y. Kim, C. Kim, I. Choi, S. Rengaraj, J. Yi, *Environ. Sci. Technol.* **2004**, *38*, 924 – 931.
[5] C. K. Narula, J. E. Allison, D. B. Bauer, H. S. Gandhi, *Chem. Mater.* **1996**, *8*, 984 – 1003
[6] P. Kim, Y. Kim, C. Kim, H. Kim, Y. Park, J. H. Lee, I. K. Song, J. Yi, *Catal. Lett.* **2003**, *89*, 185 – 192.
[7] Z. Zhang, R. W. Hicks, T. R. Pauly, T. J. Pinnavaia, *J. Am. Chem. Soc.* **2001**, *123*, 1592 – 1593.
[8] R. W. Hicks, T. J. Pinnavaia, *Chem. Mater.* **2003**, *15*, 78 – 82.
[9] a) L. Pidol, D. Grosso, G. J. de A. A. Soler-Illia, E. Crepaldi, P. A. Albouy, H. Amenitsche, P. Euzen, C. Sanchez, *J. Mater. Chem.* **2002**, *3*, 557 – 564; b) N. Idrissi-Kandri, A. Ayral, M. Klotz, P.-A. Albouy, A. El Mansouri, A. Van der Lee, C. Guizard, *Mater. Lett.* **2001**, *50*, 57 – 60.
[10] a) F. Schüth, *Chem. Mater.* **2001**, *13*, 3184 – 3195; b) J. Cejka, P. J. Kooyman, L. Vesela, J. Rathousky, A. Zukal, *Phys. Chem. Chem. Phys.* **2002**, *4*, 4823 – 4829; c) V. González-Peña, I. Díaz, C. Márquez-Alvarez, E. Sastre, J. Pérez-Pariente, *Microporous Mesoporous Mater.* **2001**, *44–45*, 203 – 210; d) S. Rana, S. Ram, *Phys. Status Solidi A* **2004**, *201*, 427 – 444; e) X. Zhang, F. Zhang, K.-Y. Chan, *Mater. Lett.* **2004**, *58*, 2872 – 2877.
[11] S. Vaudreuil, M. Bousmina, S. Kaliaguine, L. Bonneviot, *Microporous Mesoporous Mater.* **2001**, *44–45*, 249 – 258.
[12] J. M. Kim, M. Kang, S. H. Yi, J. E. Yie, S. H. Joo, R. Ryoo, *Stud. Surf. Sci. Catal.* **2003**, *146*, 53 – 56.
[13] G. J. de A. A. Soler-Illia, E. L. Crepaldi, D. Grosso, C. Sanchez, *Curr. Opin. Colloid Interface Sci.* **2003**, *8*, 109 – 126.
[14] D. Grosso, F. Cagnol, G. J. de A. A. Soler-Illia, E. L. Crepaldi, P. A. Albouy, H. Amenitch, A. Brunet-Bruneau, C. Sanchez. *Adv. Funct. Mater.* **2004**, *14*, 309 – 322.
[15] E. L. Crepaldi, G. J. de A. A. Soler-Illia, D. Grosso, F. Cagnol, F. Ribot, C. Sanchez, *J. Am. Chem. Soc.* **2003**, *125*, 9770 – 9786.
[16] D. Grosso, C. Boissière, B. Smarsly, T. Brezesinski, N. Pinna, P. A. Albouy, H. Amenitsch, M. Antonietti, C. Sanchez, *Nat. Mater.* **2004**, *3*, 787 – 792.
[17] C. Pecharroman, I. Sobrados, J. E. Iglesias, T. Gonzales-Carreno, J. Sanz, *J. Phys. Chem. B* **1999**, *103*, 6160 – 6170.
[18] A. Thomas, H. Schlaad, B. Smarsly, M. Antonietti, *Langmuir* **2003**, *19*, 4455 – 4459.
[19] A. Brunet-Brunneau, A. Bourgeois, F. Cagnol, D. Grosso, C. Sanchez, J. Rivory, *Thin Solid Films* **2004**, *455*, 656 – 660.
[20] D. Grosso, G. J. de A. A. Soler-Illia, E. L. Crepaldi, F. Cagnol, C. Sinturel, A. Bourgeois, A. Brunet-Bruneau, H. Amenitsch, P. A. Albouy, C. Sanchez, *Chem. Mater.* **2003**, *15*, 4562 – 4570.

